Motivation of the Barrel Time-of-Flight Detector for $\overline{\mathrm{P}}$ANDA

Draft 1.1

A. Gillitzer, A. Kisselev, A. Sanchez-Lorente, L. Schmitt, C. Schwarz

Abstract

This report evaluates the physics potential and technical benefits of the barrel time-of-flight detector and summarizes its requirements.

Contents

1 Introduction

This section deals with two major requirements of the $\overline{\mathsf{P}}$ANDA experiment. The first one is the need for charged particle identification (PID) over a large momentum range. This cannot be achieved with one single process but several detectors have to participate. One component of PID is the measurement of the time-of-flight of particles, which provides the velocity allowing to discriminate different masses for slower particles.

The second requirement is the online selection of interesting physics signatures from the data read out from all interactions. The first step of the selection has to be fast enough to fit to manageable online computing resources and arrive at acceptable event rates. This topic will be part of a second document.

In this section basic principles related to the time-of-flight detectors concerning the above mentioned requirements are explained.

1.1 Positive Particle Identification

A critical issue is the evaluation of particle identification requirements of physics topics relevant for $\overline{\mathsf{P}}$ANDA. Here two applications have to be distinguished:

Positive particle identification means to identify a particle as being of the type required for a given physics channel and distinguish it like this from all other particle hypotheses. This method is needed in cases where a large background completely covers the looked for signal exceeding it often by many orders of magnitude. As a particular example in many cases pions are much more abundant than Kaons and if a channel containing a Kaon cannot be tagged by other means identifying the Kaon is the most important tool to select the signal.

Negative particle identification means to identify a particle as being of another type than the one required for a given physics channel and like this reject particles belonging to the background. This method allows to improve an already selected signal by enhancing the signal-to-background ratio but fails in the primary selection. Again the example of pions vs. Kaons illustrates this: If the presence of a Kaon is required to select the signal, deselecting an event where a pion was identified is not sufficient. Typical misidentification rates are of the order of up to a percent. If a background rejection of several orders of magnitude is required the misidentified pions interpreted as Kaons still lead to a far too large background to clearly prepare the signal.

The effect of completely covering a very small signal by a small but still not negligible misidentified background is illustrated in Fig. 1. In simulations performed for the Conceptual Design Report of FAIR [2] at low momenta a misidentification level of pions of about 0.5 % was found, consistent with previous results from BaBar.

1.2 Algorithms for Relative Time-of-Flight

ToF-based PID at PANDA is significantly complicated by two facts: The experiment will run with a continuous high-rate anti-proton beam. In addition the installation of detector(s) with very good time resolution close to the interaction point is excluded for technical reasons.

Under these conditions only the information on *relative* times of flight between charged particles in a given event is available, and clearly a "conventional" single-track-based PID can not be applied. There are a number of methods used to deal with the ToF-based PID in such a configuration, which were described in detail elsewhere (see for instance presentation

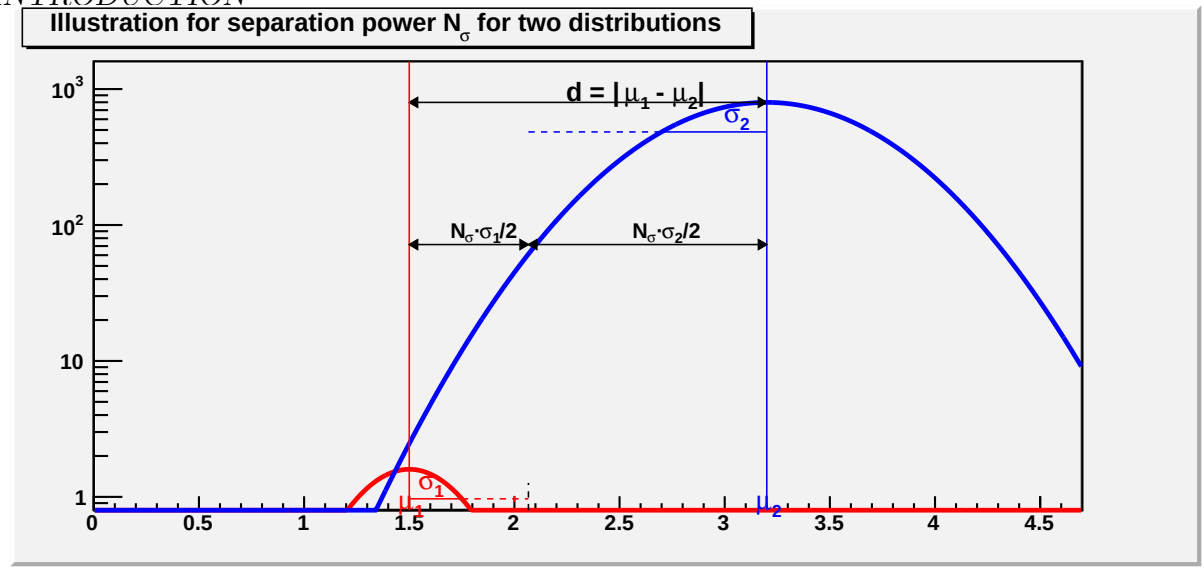

Figure 1: Separation power in a situation where the background is 1000 times higher than the signal. Even if the background can be identified, a small percentage of misidentified particles can fully cover the signal. Note the logarithmic vertical scale.

by S.Spataro for the XXVI PANDA meeting in Ferrara in 2008 [3]). Here we cover them only briefly.

1.2.1 One identified particle in event

In case one of the particles in a given (multi-track) event is identified by means of some other PID detector(s), one can use its measured arrival time t, momentum p, path length L between the production vertex and the registering detector and mass hypothesis m in order to estimate the start time (t_S):

$$t_S = t - L\sqrt{p^2 + m^2}/(pc) \tag{1}$$

and use this information about t_S to identify other particles in the event, assuming that the time-of-flight ToF_i for a given i-th particle with a measured arrival time t_i equals to $ToF_i = t_i - t_S$.

1.2.2 Few identified particles in event

In case more than one particle in a given event was identified by other PID detectors, one can calculate a weighted mean of their t_S estimates in order to improve the accuracy. The task is equivalent to finding a minimum of the functional $\Psi^T(t_S)$, which (neglecting uncertainties in momentum and path length estimates and accounting for arrival time measurement errors σ_{Ti}) can be written down as a quadratic form with respect to t_S:

$$\Psi^T(t_S) = \sum_i \frac{(t_i - L_i\sqrt{p_i^2 + m_i^2}/(p_i c) - t_S)^2}{{\sigma_T}_i^2}, \tag{2}$$

where the sum is taken over all the *identified* particles, and be easily solved. Once t_S is found in this way, ToF-based identification of the other charged particles in event proceeds the same way as described in 1.2.1.

1.2.3 Simultaneous start time and particle mass variation

As a variant of 1.2.2, but without having any external PID knowledge on some of the particle types in event one can try to construct a different t_S-dependent functional

$$\Psi^M(t_S) = \sum_i (m_i(t_S, t_i, p_i, L_i) - m_i^0(t_S))^2, \tag{3}$$

where the sum is now taken over *all* charged particle tracks with the arrival time measurement t_i available, $m_i = p_i\sqrt{(t_i c)^2/l_i^2 - 1}$. A step-wise quantity $m_i^0(t_S)$ for each of the tracks in the above Ψ^M-functional is a closest to $m_i(t_S)$ value of a "realistic" particle mass out of the discrete set of values $\{m_e, m_\pi, m_\mu, m_K, m_p\}$. Written down like this, $\Psi^M(t_S)$ is a piece-wise smooth function of t_S and its global minimum can be taken as the best guess t_S estimate. Once t_S is found in this way, a set of $\{m_i^0\}$ values at this t_S can be used as "identified" particle mass hypotheses.

1.2.4 Other ideas

Each of the options presented above has certain drawbacks. The first two methods require external PID input. The latter one works in mass space, where error estimates are no longer gaussian, so the χ^2-like formulation of Eq. (3) is questionable. Neither of the presented options takes momentum measurement uncertainties into account. Also they do not provide any means to *quantify* the PID decision, so a detailed Monte-Carlo for a given physics channel is needed to estimate the efficiency and contamination by other particle types.

An attempt to overcome part of these difficulties has been taken recently [4]. For a given N-track event and in general M possible particle mass hypotheses (see 1.2.3, where M is taken to be 5) the suggested technique gives a statistically correct evaluation of all the M^N possible particle mass configurations by providing a χ^2 probability weight $W_{\{m_1,...,m_N\}}$ for each of them. In a simplified formulation the task to evaluate a certain particle mass configuration $\{m_1, ..., m_N\}$ for a given event is reduced to the minimization of a functional very similar to the one considered in subsection 1.2.2:

$$\Psi^T_{W_{\{m_1,...,m_N\}}}(t_S) = \sum_i \frac{(t_i - L_i\sqrt{p_i^2 + m_i^2}/(p_i c) - t_S)^2}{{\sigma_T}_i^2 + {\sigma_R}_i^2}, \tag{4}$$

where the sum however is taken now over *all* tracks with the time-of-flight measurement and the denominator for each term is properly expanded by additional uncertainty coming from momentum and path length reconstruction errors σ_{Ri}. For the "true" particle mass configuration the quantity $\Psi^T_{W_{\{m_1,...,m_N\}}}$ at the minimum vs t_S should be distributed as χ^2 with $N-1$ degrees of freedom. Therefore it makes perfect sense to use a probability of observing obtained χ^2 value as a weight $W_{\{m_1,...,m_N\}}$ for a given mass configuration. The unique "true" configuration will have a flat distribution of this quantity in the range [0..1], all the others - the "wrong" ones - will tend to have higher χ^2 values and peak close to 0 depending on how incorrect their mass hypotheses are.

In principle a set of M^N weights $W_{\{m_1,...,m_N\}}$ contains all the information provided by the tracking and time-of-flight subsystems, which can be used for a PID decision. The way of usage depends on the layout of the global PANDA PID. In particular, a set of weights $W_{\{m_1,...,m_N\}}$, together with the t_S estimates for all the considered particle mass configurations can be given over to this global PID as input.

Alternatively, a "standalone" PID mode is possible. For example, a decision on a probability for a given j-th particle to be a pion can be formulated as

$$\epsilon_j^\pi = \frac{\sum_{\{j\}=\pi} W_i}{\sum_{i=1}^{M^N} W_i}, \tag{5}$$

where the sum in the numerator is taken over all particle mass configurations, where the j-th particle was assumed to be a pion, and the sum in the denominator is taken over all M^N configurations. The closer the quantity ϵ_j^π is to 1, the larger is the probability that the particle was a pion, in this particular case. The value of ϵ_j^π in this example can therefore be taken as selection criterion to either accept ($\epsilon_j^\pi \geq \epsilon_{min}$) or discard ($\epsilon_j^\pi < \epsilon_{min}$) a given track as a pion. The preliminary results of PYTHIA Monte-Carlo at 10 GeV/c beam energy for PANDA Forward Spectrometer are shown in Fig. 2 for different momentum ranges. Typical events accounted on this plot have between 2 and 4 charged tracks in forward direction. Arrival time resolution of the Forward ToF Wall is assumed to be $100ps$ for each track. ϵ_{min} cut value varies between 0.1 and 0.9 along each of the four coloured lines, for illustrative purposes. One can see for instance, that at 3 GeV/c momentum (blue curve) ϵ_{min} cut can be selected such, that pions will be identified correctly in $\sim 98\%$ of cases, at a price of $\sim 5\%$ of protons misidentified as pions.

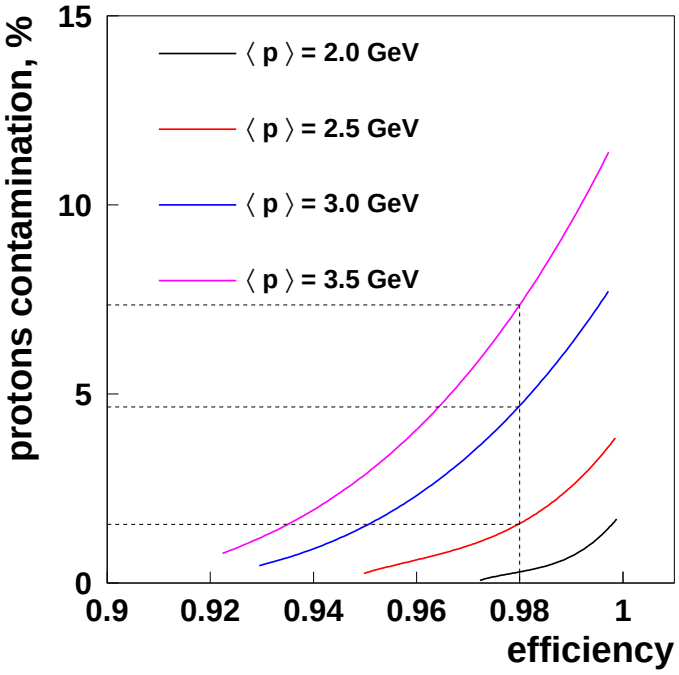

Figure 2: Proton contamination versus pion selection efficiency as a function of ϵ_j^π.

Probabilities of multi-particle subsets of a given event can be evaluated in a similar fashion. If some of the particles were reliably identified by the other PID detectors, respective weights for "wrong" configurations should be explicitely set to 0 prior to calculating the probabilities of Eq. (5). Such "external" input should also reduce the significant combinatorial CPU overhead, intrinsic to this method.

A more sophisticated formulation of the described formalism allows to take into account the χ^2 value of the Kalman-filter-based track parameter fitting procedure, and make use of the limited timing capabilities of straw tracking detectors.

It should be stated explicitely, that the suggested PID algorithm uses all the charged particle tracks of a given event at once, no matter whether they were registered by the Target or Forward Spectrometers. The predictive power of the PID decision is the better, the more tracks with different topologies and high-resolution ToF measurement are taken into account. In particular, availability of the tracks with Barrel ToF information should drastically improve the ToF-based PID procedure quality for the configurations with only a few tracks in the forward direction, and also make possible such a PID for the large class of events with only a single charged particle track in the Forward Spectrometer.

2 Physics Case

2.1 Hypernuclei

Hypernuclear research will be one of the main topics addressed by the $\overline{\mathsf{P}}$ANDA experiment [23] at the planned Facility for Antiproton and Ion Research FAIR [24]. The $\overline{\mathsf{P}}$ANDA hypernuclear programme shall reveal the strength of Λ–Λ interaction via the high resolution γ spectroscopy of double Λ hypernuclei. Contrary to past hypernuclear experiments, where only a few double hypernuclei events were found, the challenge of the $\overline{\mathsf{P}}$ANDA experiment will be the enhancement in statistics with an order of magnitude five larger than in previous experiments. The reason resides in the fact that germanium detectors, instead of their good energy resolution, have an efficiency of only a few percent.

In combination with a high luminosity of the antiproton beam at HESR, a high production rate of single and double hypernuclei under unique experimental conditions will be possible by the first time.

In the $\overline{\mathsf{P}}$ANDA experiment, double hypernuclei will be produced as a result of a multi–stage process. In the first stage a Ξ^- (together with its associated strange particle) is produced in a primary target via the $\overline{p} + p \rightarrow \Xi^-\overline{\Xi}^+$. The $\overline{\Xi}$ will undergo scattering or (in most cases) annihilation inside the residual nucleus. Strangeness is conserved in the strong interaction and the annihilation products contain at least two anti-kaons that can be used as a tag for the reaction.

In a second stage, the Ξ^- is slowed down in a dense, solid material (e.g. a nuclear emulsion) and forms a Ξ^- atom [7]. After an atomic cascade, the hyperon is finally captured by a secondary target nucleus. If the momentum of the hyperon is too high its stopping time will exceed the lifetime and hence the Ξ^- will decay prior to the atomic capture with high probability. In order to reach a high capture probability it is mandatory to keep the primary momentum of the produced Ξ^- as low as possible.

The energy release of about 28 MeV during the conversion of the Ξ^- into two Λ hyperons may give rise to the emission of particles from the nucleus (*double* Λ *compound nucleus*), where the conversion took place. As a consequence, a variety of double, single or twin hypernuclei as well as ordinary nuclei may be produced in excited states.

The hypernuclei study will make use of the modular structure of the $\overline{\mathsf{P}}$ANDA detector. Removing the backward end-cap calorimeter will allow to add a dedicated nuclear target station and the required additional detectors for γ spectroscopy close to the entrance of $\overline{\mathsf{P}}$ANDA.

The major difficulty to accomplish this project resides in the complexity of the hypernuclei production mechanism and in the identification procedure. Furthemore, the $\overline{p}p \rightarrow \Xi^-\overline{\Xi}$ cross section of 2μb is about a factor 25000 smaller than the total $p\overline{p}$ cross section of 50 mb at 3 GeV/c. As a consequence an strategy must be performed to enable an efficient background signal suppression. As it was remarked before, associated antihyperons annihilates with a

large probability[1] ($\simeq 85\%$) within the primary target nucleus releasing at least two positive kaons which can be used to tag the hypernuclei production. Kaons produced in this way are emitted in the forward direction (beam direction) and with a momentum distribution around 500 MeV/c. Here the difficulty resides in finding a proper detector system to identify efficiently positive kaons.

Due to the importance of this aim, the present chapter is devoted to introduce a strategy for background rejection based on the positive kaon identification, which must help to tag the production of double Λ hypernuclei at $\overline{\mathsf{P}}$ANDA. The kaon identification method presented here, contemplates the use of the time measurement.

In the current $\overline{\mathsf{P}}$ANDA design, particle identification for slow particles (below 700 MeV/c) may be provided at large polar angles by a Time Of Fight detector in combination with the Time Projection Chamber (TPC).

In the following, the efficiency of this technique will be studied by means of Monte Carlo calculations.

2.1.1 Rate estimate

Based on calculations, the various steps of the double hypernucleus production process have been quantified in order to derive an estimate of the final count rate.

According with these calculations, the rate estimate is based on an antiproton interaction rate of $3 \cdot 106\,\mathrm{s}^{-1}$. At a $\overline{\mathrm{p}}$ momentum of 3 GeV/c the $\overline{\mathrm{p}}\mathrm{p} \to \Xi^-\overline{\Xi}^+$ production cross section is about 2 μb [8], to be compared to the elastic cross section $\sigma_e(\overline{\mathrm{p}}\mathrm{p} \to \overline{\mathrm{p}}\mathrm{p}) \approx 23.7$ mb and the annihilation cross section of $\sigma_a(\overline{\mathrm{p}}\mathrm{p} \to X) \approx 26$ mb. Since no information on the mass dependence of the $\Xi^{-,0}\,\overline{\Xi}^+$ production cross section is available, we assume a $A^{2/3}$ dependence. This results in $\sigma(\Xi^{-,0}\,\overline{\Xi}^+)/\sigma_{tot} = 4 \cdot 10^{-5}$. With these assumptions we expect approximately 100 $\Xi^-\overline{\Xi}^+$ pairs per second or 11 million per day. For a target in the Carbon mass region the "production factor" (PF) is of the order $7.5 \cdot 10^{-3}$. This provides with about 64 800 stopped Ξ^- per day.

Assuming a $\Xi^-\mathrm{p} \to \Lambda\Lambda$ conversion probability of only 5 %. This results in the production of about 3 240 double hypernuclei per day.

Individual excited states may be populated with up to 10 % of the total yield [13]. From the thickness of the secondary target and the neutron moderator we estimate for γ energies between 0.1 and 10 MeV an escape probability of a gamma ray from the target between 60 and 80 %. One cluster detector mounted at a distance of 30 cm covers 0.79 % of 4π. Since the decaying hypernuclei are at rest and assuming isotropic angular distributions, 15 cluster detectors will cover approximately 11.8 % of 4π corresponding to a full photo-peak efficiency of 2.75 % for 1.33 MeV γ-rays.

The proposed trigger scheme assumes a detection of hadrons containing the associated anti-strange quarks. The cleanest tag will be a high momentum $\overline{\Xi}^+$ at small angles. However, the majority of $\overline{\Xi}^+$ will annihilate in the primary nucleus. Assuming the $\overline{\Xi}^+\mathrm{p}$ absorption cross section to be close to the $\overline{\mathrm{p}}\mathrm{p}$ annihilation cross section and averaging over the impact parameter we expect even in case of a carbon target a $\overline{\Xi}^+$ escape probability of only 20 %.

The expected reconstruction efficiency is about 40 %. This value has been estimated by considering that the geometric acceptance of the proposed layout for positive kaon identification emitted into the forward beam direction is of the order of 70%, a tracking efficiency (accepted tracks candidates by the tracking procedure) of the 60 % and the particle identification efficiency is of the 95% percent taking into account a time resolution of 100 ps for the start detector.

[1] Probability is given by the UrQMD model

While two kaons will be produced in the annihilation process, the trigger will be based on the detection of only one K^+ in the forward region $\theta \leq 40°$ not covered by the secondary target. In order to reduce the single K^+ rate of about $5 \cdot 10^5\,\mathrm{s}^{-1}$ to a rate acceptable by the DAQ, additional filters based, for example, on the vertex in the secondary target, the signals in the Germanium detectors or the missing energy in the forward region will be employed. In the present work, a kaon trigger efficiency between 20 % and 30 % has been achieved. However, an efficiency of about 40% would be a desirable aim.

In conclusion, the expected rate after the use of the kaon trigger is of about 69 events per month for an individual transition (See Table 1).

The rate estimates corresponding to the UrQMD+SMM calculations are in comparison with previous calculations (Intra nuclear casacde (INC) generator interface) a factor of 10 larger.

$\overline{\mathrm{p}}$ interaction rate	$3 \cdot 10^6\mathrm{s}^{-1}$
$\overline{\mathrm{p}}$ momentum	$3\,\mathrm{GeV}/c$
internal target	$Z \approx 6$
reactions of interest	$\overline{\mathrm{p}}\mathrm{p} \rightarrow \overline{\Xi}^+\Xi^-$
	$\overline{\mathrm{p}}\mathrm{n} \rightarrow \overline{\Xi}^+\Xi^0$
cross section ($\overline{\mathrm{p}}N$)	$2\,\mu\mathrm{b}$
rate	$100\,\mathrm{s}^{-1}$
Ξ^- PF	$7.5 \cdot 10^{-3}$
total stopped Ξ^-	64 800 per day
$\Xi^-\mathrm{p} \rightarrow \Lambda\Lambda$ conversion probability	5 %
produced $\Lambda\Lambda$ hypernuclei	3 240 per day
probability of individual transition	10 %
target escape probability ($E_\gamma = 1\,\mathrm{MeV}$)	70 %
Ge solid angle	11.8 %
Ge efficiency ($E_\gamma = 1.33\,\mathrm{MeV}$)	23.3 %
trigger efficiency	20–30 %
detected individual transitions	69 per month

Table 1: Rate considerations for hypernuclear physics with γ-ray spectroscopy. An event generator based on a intra nuclear cascade model was used for $\overline{\mathrm{p}}\mathrm{p} \rightarrow \overline{\Xi}^+\Xi^-$ generation.

2.1.2 Generation of Hypernuclei

The Monte Carlo calculations will make emphasis on the first stage of the hypernuclei mechanism, which regards the generation of $\Xi^- + \overline{\Xi}^+$ pairs in the $\overline{p}$+^{12}C reaction at 3 GeV/c within the primary target of the hypernuclear setup(See [23]).

For that, a primary generator (UrQMD+SMM) [10] based on an extended version of the UrQMD model [9] has been used. In this event generator, the rescattering mechanism plays a important role in the production of low momenta Ξ^- below 500 MeV. The annihilation of the associate particle $\overline{\Xi}^+$ with a nucleon, which results in at least two positive kaons, is also considered. Mandatory for this study is the production of background reactions, which correspond to $\overline{p}$+^{12}C which does not lead to the production of $\Xi^- + \overline{\Xi}^+$ pairs. The interface to the standard UrQMD model has been considered to accomplish this task.

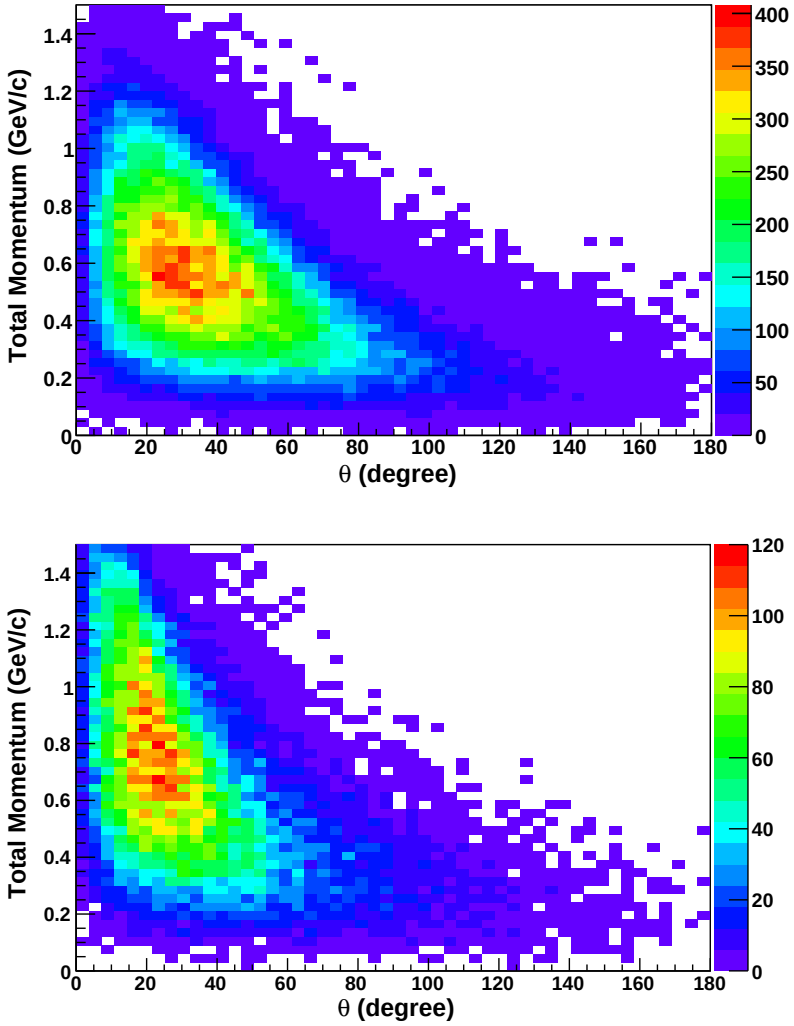

Figure 3: Phase space distributions corresponding to positive kaons produced as a result of the signal (top panel) and background (bottom panel) generation.

In the following, we will focus on the production of positive kaons, resulting from the signal and the background generation. Fig. 3 illustrates the phase space distribution of positive kaons resulting from the signal generation (top panel) and from the background generation (bottom panel), respectively. In both cases positive kaons are emitted mainly into the forward direction. However, the position of the maximum of the kaon distribution is different in each case. For example, in the case of kaons produced from the signal, the maximum is centered around 500 MeV/c and in the background case, kaons are centered around 700 MeV/c.

2.1.3 Event Simulation

The Monte Carlo simulation has been performed within the PANDAroot [11]. The hypernuclear detector setup is the one described in ref. [22, 6].

The analysis procedure in the present work is managed by tools provided by the Rho package [12]. For each event the information obtained after the reconstruction stage is asso-

ciated to particle candidates (kaons, pions or photons) according with the particle hypothesis calculated during the particle identification process and are stored in particle lists. For the identification of complete decay chains selector applications can be applied to get access to the candidate lists and to extract information such as number of particles, total event energy or four vectors of each particle.

The different detectors electronic signals are reconstructed to build particles trajectories, whose momenta can be extracted by using a devoted tracking algorithm. The assignment of particles trajectories to a certain particle type, takes place in Sec. 2.1.4, where the energy loss and the timing measurements together with the tracking information is used to calculate particle hypotheses.

In addition, the efficiency of a method for the background rejection based on positive kaon identification will be in Sec. 2.1.5 evaluated.

2.1.4 Reconstruction

The reconstruction of charged particles trajectories uses the hits information of the several detectors involved in the simulation after the digitization process. The reconstructed trajectories, denominated also tracks candidates, are parametrized with special algorithms provided by the selected track model to obtain information such as momentum, length of the trajectory, direction etc. In this section a particular emphasis will be given to the reconstruction of the low momentum charged particles resulting from the hypernuclei production mechanism. This procedure will be mainly accomplished by the secondary active target and eventually by the scintillation fibers array. Charged particles with moderated momenta emitted into the forward direction will be reconstructed making use of the time projection chamber as main tracker detector and of the time of flight system.

Momentum resolution and low momentum particles To enable the time of flight measurement, the produced particles must have enough momenta to cross the start detector, the TPC and to arrive to the time of flight barrel (stop detector). In other words, produced particles must be able to traverse the interior of the target spectrometer (radius R$\simeq$ 50 cm).

With $P_T = 0.3RBq$, positive charged kaons moving in a magnetic field B of 2 T must have a transverse momenta component P_T above 150 MeV/c to fulfil this requirement. It is also important to remark, that for a good suppression of the background signal, the detector acceptance for kaon detection has to be large. The reason for that, is that one should not only account for the probability of producing Ξ^-, but also one should consider the stopping probability and the conversion probability which represents a 5% of the total rate. The enhancement in statistic can be easily achieved by reducing the magnetic field to 1 T. As a consequence, the number of positive kaons fulfilling the above condition is then even larger, and the momentum threshold can be then placed below 100 MeV/c.

Charged Particle Identification Good particle identification (PID) for charged hadrons and leptons plays an essential role for $\overline{\mathsf{P}}$ANDA and must be guaranteed over a large momentum range from 200 MeV/c up to approximately 10 GeV/c. Several subdetectors provide useful PID information for specific particle species and momenta. While energy loss measurements within the trackers obtain good criteria for the distinction between the different particle types below 1 GeV/c, the DIRC detector is the most suitable device for the identification of particles with momenta above the Cerenkov threshold, eg. 500 MeV/c for kaons. Moreover, in combination with the tracking detectors, the EMC is the most powerful detector for an efficient and clean electron identification, and the Muon detector is designed for

the separation of muons from the other particle species. The best PID performance however can be obtained by taking into consideration all available information of all subdetectors.

The PID procedure is divided in two different parts. In the first stage the recognition is done for each detector individually, so that finally probabilities for all five particle hypothesis (e, μ, π, K and p) are provided. The probabilities are normalized uniquely by assuming same fluxes for each particle species.
In the second stage the global PID combines this information by applying a standard likelihood method. Based thereon, flexible tools can be used which allow an optimization of efficiency and purity, depending on the requirements of the particular physics channel. Based on the likelihoods obtained by each individual subdetector the probability for a track originating from a specific particle type $p(k)$ can be evaluated from the likelihoods as follows:

$$p(k) = \frac{\prod_i p_i(k)}{\sum_j \prod_i p_i(j)} \ , \tag{6}$$

where the product with index i runs over all considered subdetectors and the sum with index j over the five particle types e, μ, π, K and p.

In the following, special emphasis will be made to explain the particle identification techniques for the low and moderate momentum particles (pions, protons and kaons) emitted during the hypernuclei production. Basically the techniques here employed are the use of dE/dx and the timing measurements by the secondary active target and the TOF detector system respectively. Due to the readout electronics similarity between the secondary active target and the MVD readout electronics, the technique relative to dE/dx measurement performed by the latter will be also here adopted.

Using the tracking (momentum, charge, track length) and the timing information particle identification may be performed. Indeed, a particle with mass m and momentum p has a velocity v which can be expressed in units of the light velocity c by $\beta = v/c$

$$\begin{aligned} \beta &= \frac{p}{\sqrt{p^2 + m^2}} \\ \gamma &= \frac{1}{\sqrt{1 - \beta^2}} \end{aligned} \tag{7}$$

Using the definition of γ and β, one gets the following expression $\frac{p}{m} = \beta\gamma$.

Based on this feature, different methods can be adopted for particle identification (PID). In the following, the so–called "probability method" will be reviewed.

Probability method The probability method consist in assigning to each kind of particle a probability density function (p.d.f.) based on some separation parameter, for instance the mass, by fitting the appropriate Monte Carlo simulated distribution. Therefore, one can compute the probabilities for each track, measured with a given mass m, to be a pion, a kaon or a proton from the heights of the corresponding mass p.d.f's (f_k, f_π, f_p) at this m–value. Each p.d.f. should be normalized to the corresponding particle yield. The probability to be a particle of type i can be indeed defined as

$$P_i(m) = \frac{f_i}{f_\pi(m) + f_k(m) + f_p(m)} \tag{8}$$

Fig. 4 shows an example of the p.d.f, for $i = k, \pi, p$, obtained as Monte Carlo mass distributions. However, mass is not a very good separation parameter because its probability density function has not a proper Gaussian shape as a consequence of the mass determination. Time–of–Flight is indeed Gaussianly distributed and can be more conveniently used

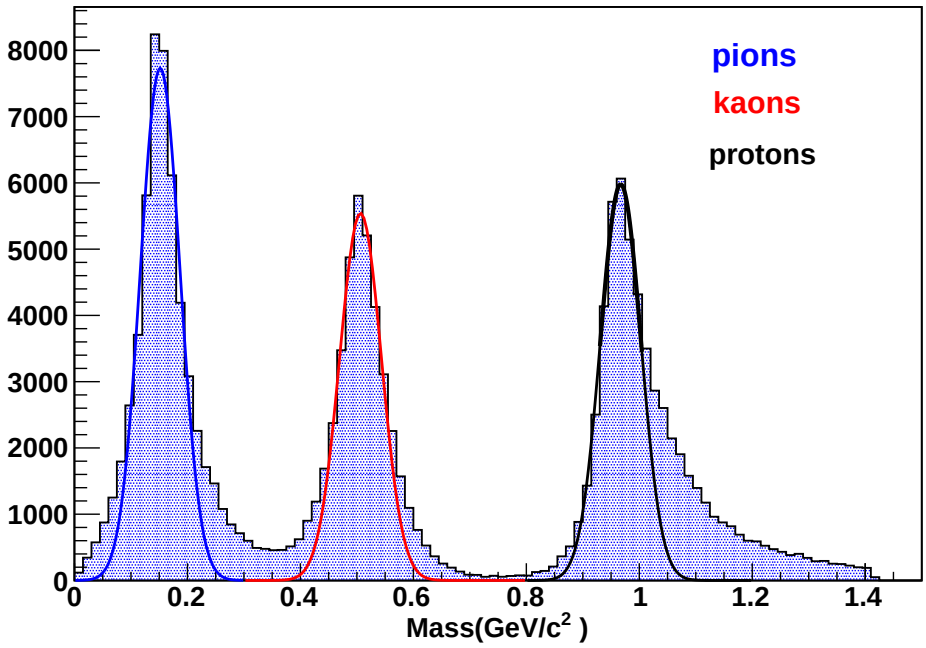

Figure 4: Mass probability density functions for pions, kaons and protons, obtained as mass spectra of unambiguously TPC–TOF matched tracks with a momentum ranging from a 200 MeV/c to 1.4 GeV/c (data sample contains 200,000 $\Xi^- + \bar{\Xi}^+$ events at B=1 T). Superimposed, some gaussian fits to guide the eye.

for probability calculations. For a track measured with a given flight–time t, the probability to have a mass m_i can be calculated for $i = k, \pi, p$ as

$$P_i(t) = \frac{g_i}{g_\pi(m) + g_k(m) + g_p(m)} \tag{9}$$

where $g(t_i)$ is the height of the Gaussian p.d.f. $g($ with mean value t and standard deviation $\sigma_t)$ at the time t_i derived from the track length l and momentum measurements with mass hypothesis m_i(see Fig. 5). Here a weighting procedure is applied to consider the different particle yields. The time–based probabilities obtained in this way are shown in Fig. 6 as functions of the mass. One can see the masses at which the probability for a particle to be a pion becomes equal to the probability to be a kaon($\equiv 0.3\,\mathrm{GeV}/c^2$), and the probability to be a kaon becomes equal the probability to be a proton($\equiv 0.7\,\mathrm{GeV}/c^2$) correspond to the crossing points of the π, K, p mass p.d.f's of Fig. 4.

2.1.5 Kaon identification based on timing measurements

In the present work, a strategy will be introduced to identify low and moderate momentum kaons via the timing measurement of TOF (Time of flight system) in combination with the tracking performance of the TPC detector at $\overline{\mathrm{P}}$ANDA. The efficiency of tagging the production of Ξ^- hyperons via the kaon identification will depend also of the geometrical acceptance of the detection system. The main difficulty of the proposed setup resides in to optimize the distance of the hypernuclear target to the central tracker of $\overline{\mathrm{P}}$ANDA spectrometer. Due to

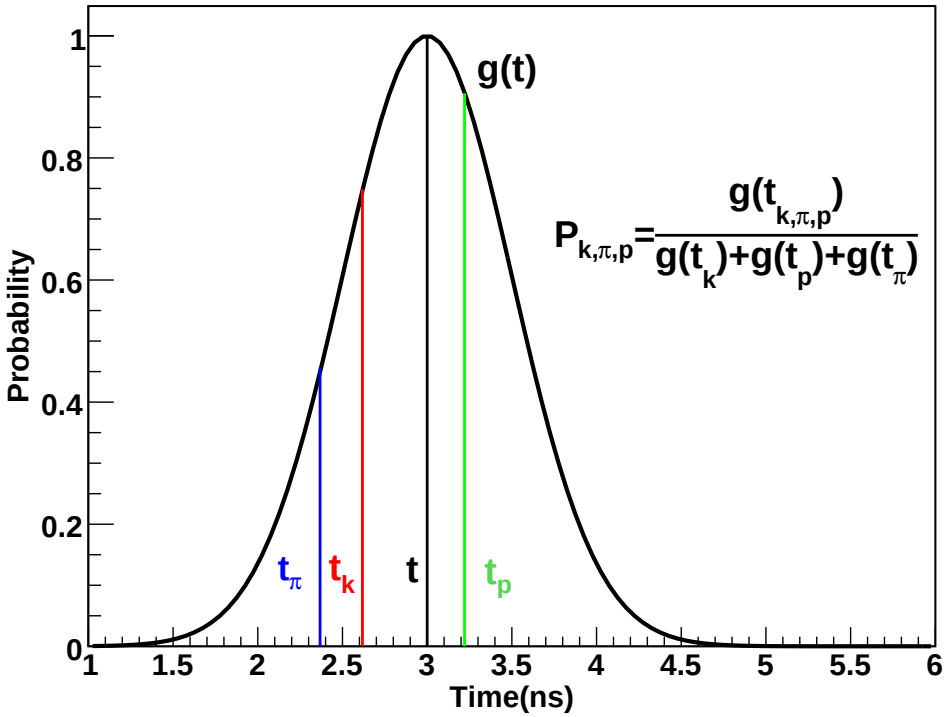

Figure 5: Example of time–of–flight probability density function. The standard deviation σ_t of this gaussian function, centered at the measured track time t, has been enlarged by an arbitrary factor for the sake of clarity.

the fact, that the backward region has been chosen for the placement of electronics readout of the central tracker detectors, the space left closed to the TPC detector is therefore limited.

The identification procedure consist in using the timing measurement, provided by the TOF detector system in combination with the tracking information given by the TPC (as discussed in Sec. 2.1.4), to separate different particles types. Moreover, the probability method, explained in Sec. 2.1.4 of this chapter, will be used to calculate the corresponding particle hypotheses, through which kaons, pions or protons will be recognized.

The starting point of the analysis begins with the production of 200,000 $\Xi^- + \bar{\Xi}^+$ pairs events at the magnetic field of 1 T by the extended UrQMD+SMM generator interface.

In the next stage, track candidates are built using the method introduced in Sec. 2.1.4. For that, hits produced in the start detector, the TPC and scintillation barrel detector are considered. Particles tracks which do not fulfil this condition will be not accepted by the tracking procedure. Typically, the geometric acceptance of the scintillation barrel detector goes from 22° to 140° for an interaction point placed at center of the target spectrometer reference system. However, because the interaction point for the hypernuclear layout is placed at -55.5 cm from target spectrometer center, the corresponding geometric acceptance will be from 14° to 80° (See Fig. 7).

For the present studies, the detector system acceptance for kaon identification is then of the order of the 60% percent. Fig. 8 illustrates a typical kaon event traversing the volumes of scintillating fiber array detector, the TPC and the TOF barrel detector. The picture shows the kaon track from the front and side view. In the next step, reconstructed tracks

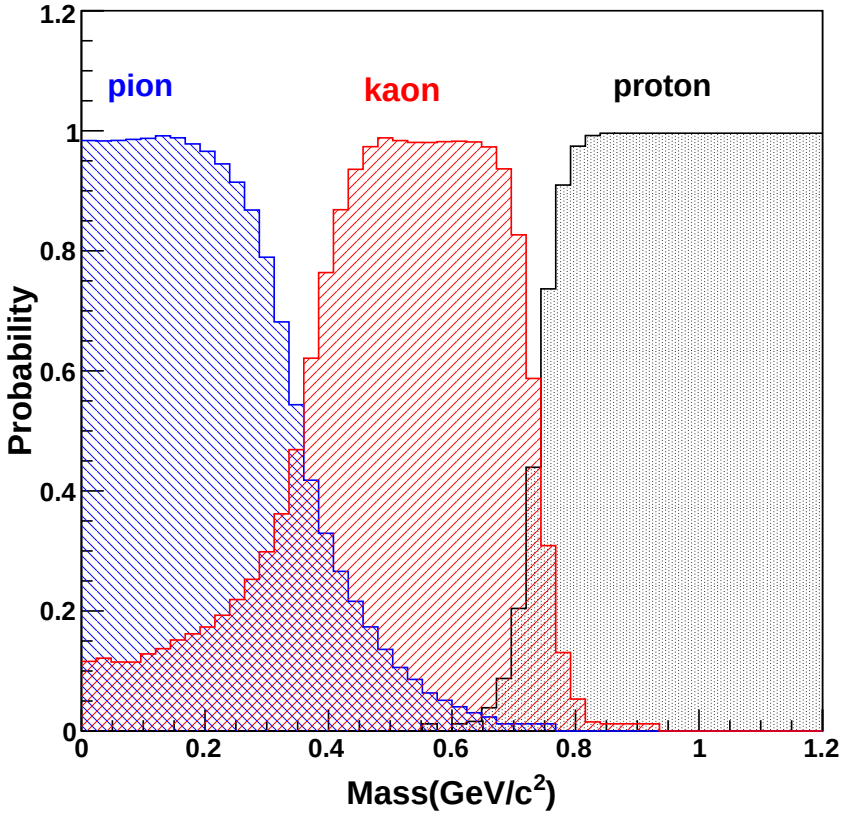

Figure 6: Time –based PID probability distributions as function of the mass, for pions, kaons and protons, corresponding to unambiguously matched TPC–TOF tracks with a momentum range from 0.3 GeV/c to 1.4 GeV/c and a track length of approximately 1 meter at B=1 T

are assigned to kaon candidates according with the particle hypotheses obtained via the probability method as indicated in Sec. 2.1.4.

To study the kaon identification efficiency the use of a start detector with a time resolution comparable with the one of the scintillator Time–Of–Flight barrel (100 ps) has been considered. Fig. 9 shows the reconstructed mass spectra assuming a start detector with 100 ps (CVD detector). One can see that for a start detector with a timing resolution comparable to the one of the TOF barrel (stop detector), particles such as pions, kaons and protons are well separated. From the tracking procedure, a momentum and the track length resolution of 1% and 3% respectively have been assumed for this analysis.

Furthermore, considering a start detector with a time resolution of 100 ps, the kaon identification efficiency [2] [3] is around the 95%.

Accordingly, the $\Xi^- + \overline{\Xi}^+$ events which can be tagged based on the kaon identification strategy is 20% (100 ps) of the total production. Assuming a timing resolution of 100 ps for both, start and stop detectors, the number of stopped Ξ^- is around 3000, which represents a 20% of the total number of stopped Ξ^- achieved by using the UrQMD+SMM generator (See Fig. 3).

[2] It is defined as the number of kaon identified by the PID system divided by the number of produced kaons
[3] assuming a kaon hypothesis larger than 0.4 (see Fig. 6)

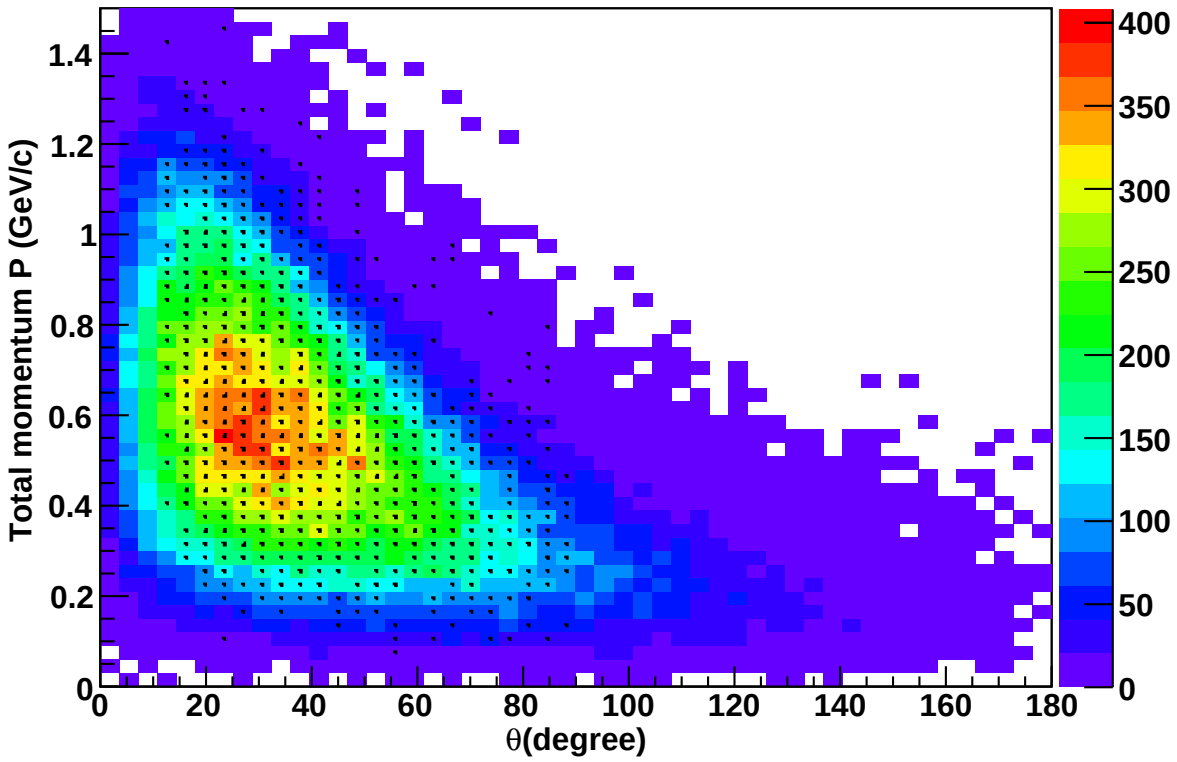

Figure 7: Scatter plot showing the geometric acceptance of the TOF barrel detector for kaons. Black boxes represent the transverse momentum vs polar angle distribution of kaon tracks which are accepted for analysis.

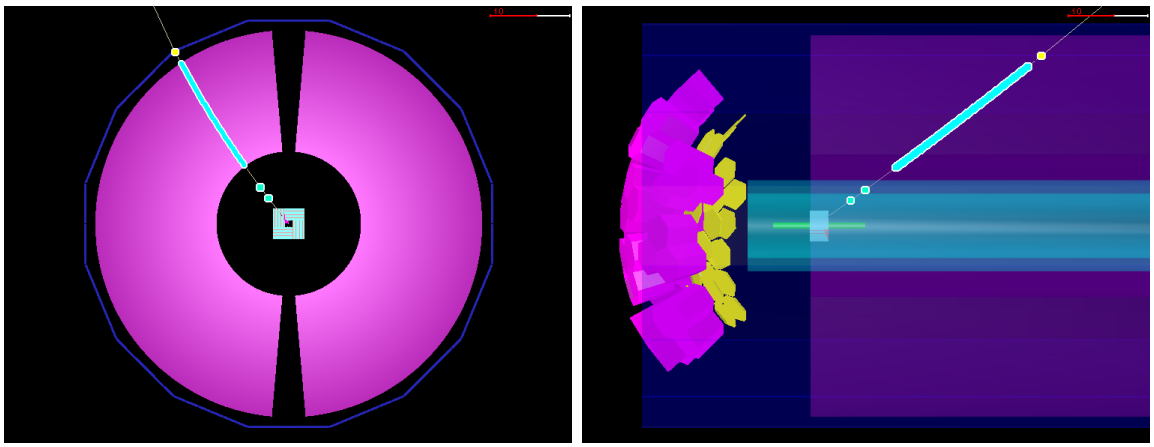

Figure 8: Left and right panel show for an IP placed at $z = -55cm$. the X-Y and Y-Z view of the TOF system layout, respectively. In both cases a kaon track is denoted by its hits on the fibers array, TPC and TOF barrel.

In addition to these calculations, the same simulation procedure has been calculated placing the hypernuclear detector layout at a distance of -55.5 cm from the center of the $\overline{\text{P}}$ANDA spectrometer. This is actually the closest distance to the central tracker the hypernuclear

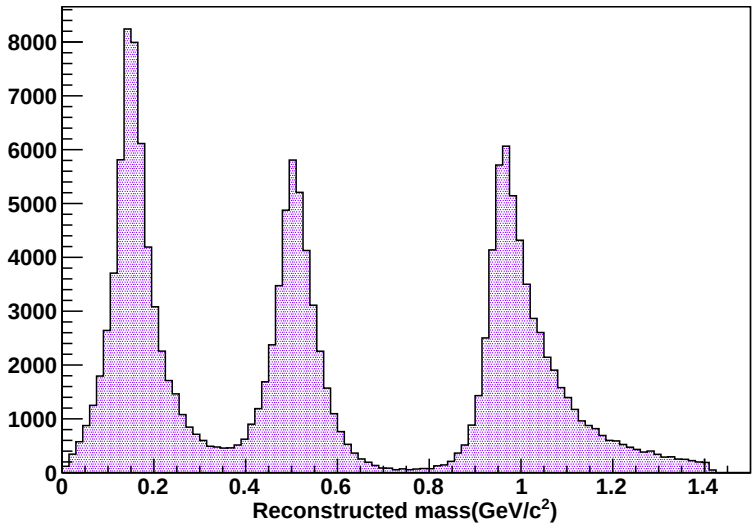

Figure 9: Mass reconstruction for positive charged pion, proton and kaons. The time resolution of TOF start detector with 100 ps. The resolution of the reconstructed momentum and length is 1% and 3%, respectively. The magnetic field value was reduced to 1 T to increase the detector acceptance.

Table 2: Efficiency of the proposed method for the tagging of $\Xi^- + \overline{\Xi}^+$ events over the background reactions ($\overline{p}$+^{12}C). The method is based on the identification of positive kaons produced as a result of the $\overline{\Xi}^+$ annihilation in the primary nuclear target

event	% at σ_t=100 ps
$\Xi^- + \overline{\Xi}^+$ (IP = -76.5 cm)	$\simeq$19.
$\overline{p}$+^{12}C (IP = -76.5 cm)	7.7
$\Xi^- + \overline{\Xi}^+$ (IP = -55.5 cm)	28.3

detector setup can be placed [14]. Nevertheless, under this condition the geometric acceptance of the TOF system should improve significantly. However, after having applied the same analysis procedure the efficiency to tag $\Xi^- + \overline{\Xi}^+$ events has a value of 28.3% considering a start detector with a time resolution of 100 ps.

Furthermore, the contamination of events resulting from background ($\overline{p}$+^{12}C) reactions can be also be estimated by applying the method explained above. Fig. 10 illustrates the reconstructed mass spectra of kaons, pions an protons particles generated as a result of $\overline{p}$+^{12}C reactions. It shows the reconstructed mass spectrum assuming a start detector with time resolution of 100 ps. The particle separation is in the case of a start detector with a 100 ps resolution not well accomplished, maybe due to the small number kaons in comparison with pions. The percentage of background events tagged considering the option of a start detector with a 100 ps time resolution is 7.7%.

Table 2 gives an overview of the efficiency of method, which has been suggested in this work, to tag the production $\Xi^- + \overline{\Xi}^+$ events over the background resulting from the $\overline{p}$+^{12}C interactions. According with previous estimates [1], a reliable trigger efficiency based on the

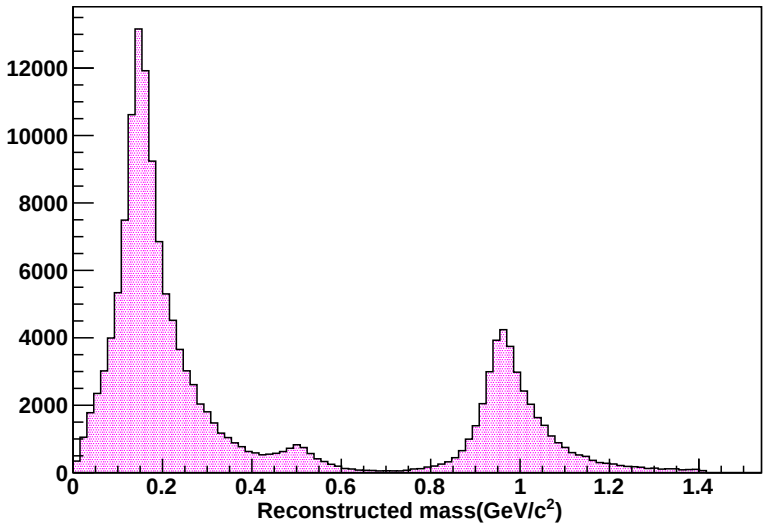

Figure 10: Mass reconstruction for positive charged pion, proton and kaons as a result of $\overline{p}$+^{12}C reactions. The resolution of the reconstructed momentum and length is 1% and 3% respectively. For this calculations a sample of 100,000 $\overline{p}$+^{12}C events have been considered.

positive kaon identification would account approximately a 40%.

Obviously, the value corresponding to the present layout is below the expected value. Furthermore, one should take into account that previous estimates have been done considering that the interaction point (IP) of the hypernuclear detector layout was placed at the center of the $\overline{\mathsf{P}}$ANDA spectrometer, where the geometrical acceptance is pretty larger that the calculated with the present layout. Actually, due to the present $\overline{\mathsf{P}}$ANDA layout it will be impossible to place the hypernuclear layout so close to the center of the $\overline{\mathsf{P}}$ANDA spectrometer.

An alternative to the present layout for background discrimination could be the use of the energy measurement of the TPC without considering the TOF system.

In summary, one can conclude that a background suppression strategy with the present considerations would be not enough as stand-alone method, and therefore it must be combined with other techniques to improve the efficiency in a factor two or more.

2.1.6 Conclusions

The associated Ξ $\overline{\Xi}$ production allows to trigger on the $\overline{\Xi}$ to suppress the background many orders of magnitude. For the planned ^{12}C primary target 15% of the $\overline{\Xi}$ leave the target and decay. The other 85% annihilate within the target and produce due to strangeness conservation two kaons. The number of positive charged kaons produced in this process amounts approximatly a 40%. Here, the reconstruction probability of the kaons is of the 28%. These results are the predictions from a URQMD+SMM model [10] containing the production of Ξ $\overline{\Xi}$ and the partial annihilation of the $\overline{\Xi}$. Background contributions to the kaon trigger amounts to 7.7% and is modelled by the URQMD model [9] not containing the above mentioned processes. Triggering on the positive kaons increase the total trigger rate by a factor of 7. The barrel DIRC can measure 55% of these kaons while 45% are below its momentum threshold. The benefit of a positive kaon identification below the momentum threshold of the barrel DIRC is a factor of 2 higher trigger rate.

2.2 Baryon Spectroscopy

The study of the excitation spectrum of baryons is an important part of the PANDA physics program. Antiproton-proton collisions are particularly well-suited to populate excited states of strange, multi-strange and charmed baryons which can be investigated in exclusive reactions. In particular, $\bar{p}p$ collisions allow independent measurements of the excitation pattern in the baryon and the antibaryon sector, which option should be exploited to significantly reduce systematic uncertainties. In order to understand the structure of individual states it is mandatory to study their coupling to different final states. These include also kaons, particularly in the decay of strange baryon resonances, as for example $\Xi^* \to \bar{K}\Lambda$ or $\Xi^* \to \bar{K}\Sigma$.

From experiments at LEAR [16] on the reaction $\bar{p}p \to \Lambda\bar{\Lambda}$ it has become evident that the angular distribution of this reaction is far from being isotropic. Instead, final states with a $\bar{\Lambda}$ in forward direction and a Λ in backward direction in the center-of-mass frame are strongly favored. The angular distribution of other hyperon production channels in $\bar{p}p$ collisions is not known, but it seems reasonable to expect forward and backward peaking of the anti-hyperon and the hyperon, respectively, also for other hyperons like Σ or Ξ, including excited hyperon states. The excited hyperon will then be slow in the lab frame and thus kaons emitted in its decay are likely to have momenta below the threshold of being identified by Cerenkov emission in the barrel DIRC detector. Qualitatively, this conclusion is correct independent of the simulation of specific reaction channels, which remains to be done in order to quantitatively determine the losses caused by the incapability to identify slow kaons.

At this point it is very important to note that the assumption of a phase space distribution in the simulation - both in the production channel and in the hyperon decay - is not suited to assess the necessity of slow kaon identification by a TOF barrel. It must be clear that the relevant criterion is *not* merely the fraction of kaons lost in the case of no TOF barrel, i.e. it is *not* a single number, but it is the question whether or not the full phase space is sufficiently covered in order to allow the measurement of complete angular distributions in production and decay channel and to determine the spin and parity quantum numbers of the excited hyperon states.

2.3 Hadrons in the Nuclear Medium

A major aspect in the study of antiproton-nucleus collisions is the question how the properties of hadrons are modified by the nuclear medium. Some hadrons may even feel a strongly attractive field such that bound nuclear states may exist. So far none of such exotic hadron-nucleus bound states caused by strong interaction has been unambiguously identified.

A particularly interesting question which has been under debate since long time is related to the possible existence of antikaonic nuclear states. This problem also has astrophysical implications as it is related to kaon condensation in compact stars. Antiproton-nucleus collisions are particularly well-suited to produce low momentum antikaons inside the nucleus which could be captured into bound states. This could be observed by using missing mass spectroscopy in the reaction $\bar{p}A \to \phi K^+ X$, based on the elementary reaction $\bar{p}p \to \phi\phi$ at small center-of-mass angles. Due to the small mass difference of ϕ and $\bar{p}$ the initial $\bar{p}$ momentum is transferred to one of the ϕ mesons whereas the other one is very low-energetic in the lab frame giving rise to a low momentum K^- captured in the bound nuclear state and a slow K^+. In case of an attractive $\bar{K}$ nuclear potential of $\sim$100 MeV in line with theoretical predictions [17] the K^+ momentum would be around 300 MeV/c.

Substantial attractive nuclear potentials have also been predicted for D mesons. The experimental investigation of D and $\bar{D}$ meson nuclear potentials is even more demanding since it requires the production of slow D or $\bar{D}$ mesons in the lab frame, respectively. Due

to the high D mass this is obviously not possible in single-step reactions. At the present stage it is not clear whether or not more complicated multi-step processes producing slow D mesons in the nuclear environment have sufficient cross section to allow unambiguous D meson identification. If this should be the case, a measurement of their transverse momentum distribution similar to the method proposed in Ref. [19]. In their decay slow D mesons would also produce kaons below the Cerenkov threshold of the barrel DIRC.

3 Further Technical Benefits

In this section various additional technical benefits are summarized briefly. The extent of their application still have to be verified and possibly simulated.

3.1 Discrimination of Charged and Neutral Particles

A fast detector sensitive to charged particles placed in the vicinity of the electromagnetic calorimeter (EMC) Covering the acceptance of the EMC can serve as input to the EMC to discriminate charged and neutral particles. This is of particular interest in the phase of software triggering when full track information is not yet available but a preselection of specific topologies requires this information. Plastic scintillators mounted in front of electromagnetic or hadronic calorimeters are used for this purpose in many hadron physics experiments.

3.2 Detection of Photon Conversions

In a similar way a fast detector sensitive to charged particles in front of the EMC can serve to detect photon conversions happening inside the other detectors. A modification of the setup where the timing barrel is placed outside the DIRC and immediately in front of the EMC would extend this capability to the detection of conversions in the DIRC, which are fairly frequent due to the thickness of the DIRC radiator. If the timing detector in addition has a reasonable spatial resolution a reliable detection and correction of the effect of photon conversions becomes possible.

3.3 Seed for Tracking

A detector with good time resolution outside the central tracker (CT) may serve as a seed for track finding in the CT. This would work best if the detector would resolve both ϕ and z at a reasonable granularity. With this combinatorics of track hypotheses in the process of pattern recognition could be reduced. This hold for both considered types of central trackers, the STT and the TPC.

In contrast, developing track seeds from the side of the MVD requires more processing time due to more complicated structure of the MVD. Moreover tracks emerging from weak decays might be missed. Another drawback here is the fact that due to the limited number of layers in the MVD many ghost tracks can be formed confusing the further steps into the CT region. Here the opposite would be applied, i.e. track seeding or at least cleaning up of tracks of the MVD by tracks from the central tracker.

Neverthless the benefits of track seeds from a high granularity timing detector would be significantly different for the two CT cases:

- In case of the straw tube tracker (STT) a 2D track seed by a timing detector can simply provide the starting point for the pattern recognition speeding up the process notably without being a fundamental ingredient.
- In the case of the time projection chamber (TPC) the tracks have the uncertainty of the starting time since the drift in t in z-direction. A 2D timing detector with segmentation in z would identify starting time of the tracks drifting within the TPC in a very easily available way allowing faster pattern recognition and more important solve the problem of event association of TPC data to the underlying interactions. No separate algorithms to find tracks from decay vertizes within the TPC would be needed.

The track seeding by the timing detector does not require the highest possible time resolution. But a key issue is to have the hits of the timing detector easily available without further parallel processing or calibration, since otherwise the tracking process would have to wait for this pre-processing. For this reason the EMC is not well suited as a detector for track seeds. In addition it can confuse charged and neutral particles.

4 Design Issues

In this section detector requirements are summarized and open design issues are discussed. One main question is the interaction with other detectors, in particular the EMC. At the end an alternative design option is presented.

4.1 Detector Requirements

The main requirement for the barrel Time-of-Flight detector is to achieve a time resolution better than 100 ps. The acceptance has to cover the angular region from 22 deg to 140 deg. The material budget of the detector has to be as small as possible. Another concern is the size of only 3 to max. 5 cm in r. To exploit further benefits the detector should have an acceptable position resolution both in z and in ϕ.

Presently three concepts are followed: One is based on long scintillator bars of 3 cm thickness arranged in a barrel shape. Two others are different designs of glass based resistive plate chambers with different readout geometry and segmentation. Here the material budge is mostly determined by the glass, the number of gaps and the number of layers. More detailed description can be found in [21].

4.2 Interaction with other Detectors

The biggest negative impact of the barrel time-of-flight detector consists in the deterioration of the response of the EMC due to photon conversions in the material of the ToF detector. The following results were presented at the PANDA Collaboration meetings in March 2010 and in September 2009 [25].

To study this G4 simulations with the Physics Book setup adding a barrel ToF detector with one layer of bars between STT and DIRC (width: 5cm, length: 190cm, inner radius: 43cm) were performed. Two settings of the barrel ToF material budget were assumed, 10%X0 as default and 20%X0 for single π^0 studies.

The material budget in front of the EMC can cause preshowers. As an example the DIRC quartz radiator with an effective thickness of 17% to 50% of a radiation length depending on the track angle had been studied previously. As a result the probability for a conversion is between 15% and 27%. The energy resolution in EMC decreases (see [26]). The barrel ToF adds material to the toal budget which will worsen the effiency.

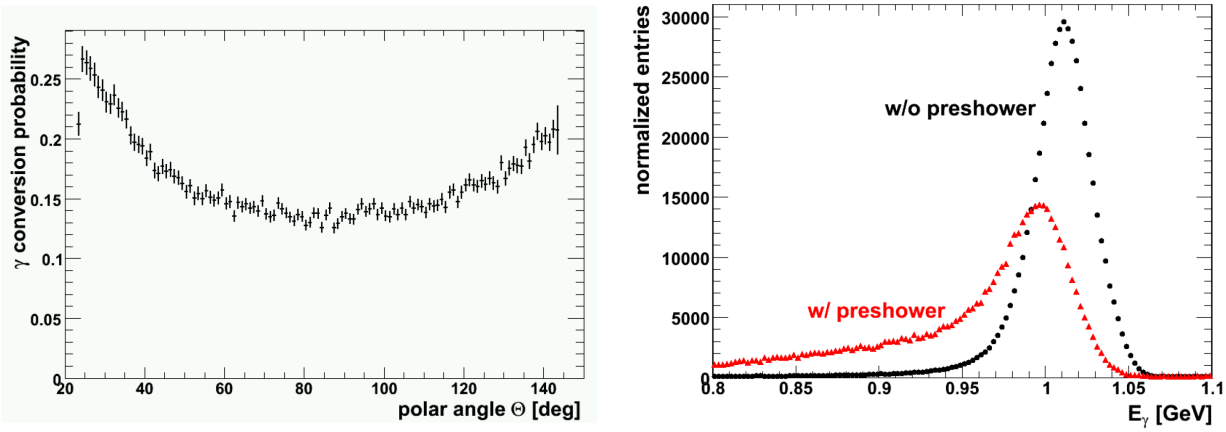

Figure 11: Preshower probability in DIRC and impact on energy resolution of EMC.

The effect of the barrel ToF on the EMC performance due additional conversions was studied with several benchmark channels.

Single π^0 were generated between 10MeV and 1.5 GeV in the barrel region and energy dependent efficiency and background studies were done. As a result an efficiency loss of 10% (20%) was found for a barrel ToF of 10% (20%) of a radiation length. The corresponding decrease in the ratio of signal to background was 20% and 40% respectively.

For the channel $p\bar{p} \rightarrow \gamma\gamma$ a reduction of S/B of 10% was found up to a value $\sqrt{s}$ of 4 GeV and 20% at 5.5 GeV.

Finally the effect on the charmed hybrid channel was studied. Here the reconstruction efficiency without ToF was 7% and with ToF 5.38%, i.e. reduced by 23 %.

4.3 Alternative Design

In this section we present a new idea for a scintillator tile hodoscope (SciTil) as general purpose timing detector in PANDA.

One of the main concerns with the barrel Time-of-Flight detectors is the influence on the EMC due to its material causing photon conversions. This effect is reduced to a minimum if one places the detector material as close as possible to the EMC and tries to reduce it to the absolute minimum. In case of the scintillator based barrel ToF the main reason for the thickness is the length of the scintillators bars leading to high light attenuation and in turn to the need for a thicker scintillator to still have an acceptable light yield. Taking all these concerns into account one arrives at a new timing detector concept based on 2x2x0.5 cm3 scintillator tiles matching the fronte face of the calorimeter crystals. The scintillator tiles are read out by SiPMs of 3x3 mm2 size. The light yield at 1 GeV (MIP) is about 50-100 detected photons. By positioning one scintillator tile 2x2 cm2 in front of each PWO crystal one achieves the shortest possible distance. The placement in the cold volume poses some additional constraints but the noise level of the SiPMs is strongly reduced. Each SiPM is read out by an ASIC so that only one five pin digital flat cables is needed for connection (2 lines differential output, one line SiPM bias, one line ASIC power and one common ground). A detector optimisation has to determine the ideal position of the SiPMs on the tiles and if one or two SiPMs per tile are needed. The ASIC will incorporate a fast preamp and a discriminator. Outside the cold volume a TDC digitizes the signals. For the SiPMs three candidates are under consideration: Hamamatsu provides so-called MPPC with $3 \times 3\text{mm}^2$ active area in a nice SMD formfactor already now. Philips has developed a Digital SiPM

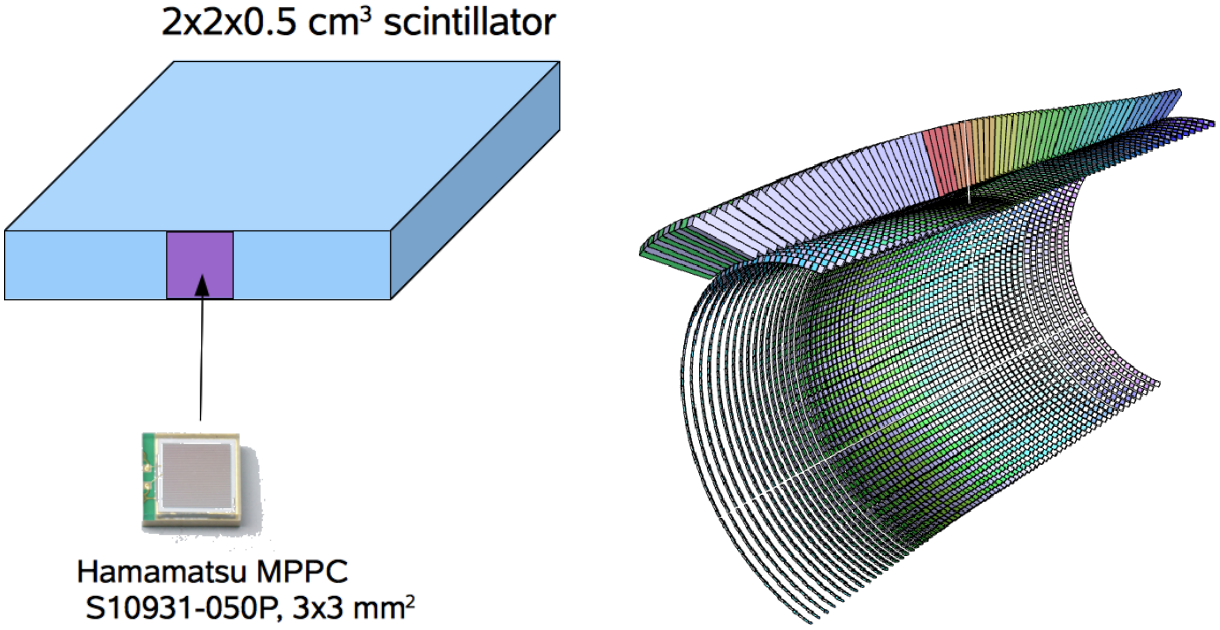

a) b)

Figure 12: Layout of the SciTil hodoscope. a) one element of the SciTil. b) A half shell of the SciTil shown with one super-module of the EMC crystals.

with on-die amplifier and TDC electronics.

The advantages of the concept are as follows: The concept results in the lowest possible material budget. It provides fast timing in the order of 100 ps for a flexible software trigger and Time-of-Flight. It allows clean detection of γ-conversions in front of the EMC in particular within the close by DIRC. In addition it is best suited for charged-neutral discrimination. If also employed in the forward endcap additional timing is available where it was previously missing altogether. Furthermore the detector provides space resolved timing signals as input to trigger metrices and TPC track finding.

The SiPM operation in the cold still has to be tested. Compared to a scintillator barrel ToF the cost is increased approximately two times. Nevertheless the R&D efforts needed for this are quite limited.

References

[1] $\overline{\text{P}}$ANDA Collaboration, Technical Progress Report, FAIR-ESAC/Pbar 2005

[2] W.F. Henning, H.H. Gutbrod, K.D. Gro, and V. Metag (editors), "An International Facility for Beams of Ions and Antiprotons (FAIR CDR)", GSI Darmstadt (2001)

[3] S.Spataro, "Time measurements without START", XXVI PANDA Collaboration meeting, Ferrara, 2008.

[4] A.Kiselev, "Yet another approach to the ToF-based PID at PANDA", XXXIII PANDA Collaboration meeting, Stockholm, 2010.

[5] H. Tamura, Phys. Rev. Lett. 84 (2000) 5963

[6] A. Sanchez Lorente, "Feasibility study of performing high precision gamma spectroscopy of $\Lambda\Lambda$ hypernuclei in the PANDA experiment", PhD Thesis, University of Mainz, August 2010.

[7] C.J.Batty, E.Friedman, A.Gal, Phys. Rev. C **59**, 295-304(1999).

[8] H. N. Brown et al, Phys. Rev. Lett**8**, (1962) 255; 257 .

[9] S. A. Bass et al., Prog. Part. Nucl. Phys. **41**, 225 (1998).

[10] A. Galoyan, Private Comunication.

[11] FairRoot, Simulation and Analysis Framework, http://fairroot.gsi.de.

[12] Rho: A Set of Analysis Tools for ROOT,http://savannah.fzk.de/websites/hep/rho/.

[13] T. Yamada and K. Ikeda, Nucl. Phys. **A585**, 79c, 1995.

[14] D. Orecchini and D. Rodriguez,Panda Collaboration Meeting, Mechanical Integration, March. 2010 Private Comunication.

[15] Resolution Studies for the Micro Vertex Detector of the $\overline{\text{P}}$ANDA Experiment and the Reconstruction of Charmed Mesons for Specific Hadronic Channels, Rene Jaekel, Phd Thesis, 2009, private communication.

[16] PS-185 reference

[17] theory references on Kbar nucleus potential

[18] theory references on D nucleus potential

[19] J. Pochodzalla, Phys. Lett. B 669 (2008) 306

[20] Wiki page of the $\bar{\text{P}}$ANDA PID TAG http://panda-wiki.gsi.de/cgi-bin/viewauth/Tagpid/WebHome,

[21] "Particle Identification at PANDA", Report of the PID TAG, March 2009, http://www-panda.gsi.de/db/notesDBr/GS14-090310_pid-tag.pdf

[22] M. F. Lutz, B. Pire, O. Scholten, R. Timmermans and W. Erni *et al.* [The PANDA Collaboration], "Physics Performance Report for PANDA: Strong Interaction Studies with Antiprotons," arXiv:0903.3905 [hep-ex].

[23] $\overline{\text{P}}$ANDA Collaboration, Technical Progress Report (GSI Darmstadt), pp. 1-383 (2005).

[24] I. Augustin, H.H. Gutbrod, D. Krämer, K. Langanke, H. Stöcker, Fourth International Conference on Fission and Properties of Neutron-Rich nuclei,Sanibel Island, Florida, 2007; arXiv:0804.0177v1 [hep-ph].

[25] B. Roth, "Pros and Cons of Barrel-ToF for PANDA", XXXII PANDA Collaboration meeting, GSI, 2010. B. Roth "Barrel TOF and Phi-Phi-Pi0 analysis", PID ToF Session at XXX PANDA Collaboration meeting.

[26] W. Erni et al. [PANDA Collaboration], "EMC Technical Design Report", October 2008, 199 pages, arXiv:0810.1216v1.